JACS
JOURNAL OF THE AMERICAN CHEMICAL SOCIETY

ARTICLE

pubs.acs.org/JACS

Dynamic Double Lattice of 1-Adamantaneselenolate Self-Assembled Monolayers on Au{111}

J. Nathan Hohman,[†,‡] Moonhee Kim,[†] Björn Schüpbach,[§] Martin Kind,[§] John C. Thomas,[†] Andreas Terfort,[*,§] and Paul S. Weiss[*,†,‡,∥]

[†]California NanoSystems Institute and Department of Chemistry and Biochemistry, and [∥]Department of Materials Science and Engineering, University of California, Los Angeles, California 90095, United States

[‡]Department of Chemistry, The Pennsylvania State University, University Park, Pennsylvania 16802, United States

[§]Institut für Anorganische und Analytische Chemie, Universität Frankfurt, Frankfurt 60438, Germany

Supporting Information

ABSTRACT: We report a complex, dynamic double lattice for 1-adamantaneselenolate monolayers on Au{111}. Two lattices coexist, revealing two different binding modes for selenols on gold: molecules at bridge sites have lower conductance than molecules at three-fold hollow sites. The monolayer is dynamic, with molecules switching reversibly between the two site-dependent conductance states. Monolayer dynamics enable adsorbed molecules to reorganize according to the underlying gold electronic structure over long distances, which facilitates emergence of the self-organized rows of dimers. The low-conductance molecules assume a (7×7) all-bridge configuration, similar to the analogous 1-adamantanethiolate monolayers on Au{111}. The high-conductance molecules self-organize upon mild annealing into distinctive rows of dimers with long-range order, described by a $(6\sqrt{5} \times 6\sqrt{5})R15°$ unit cell.

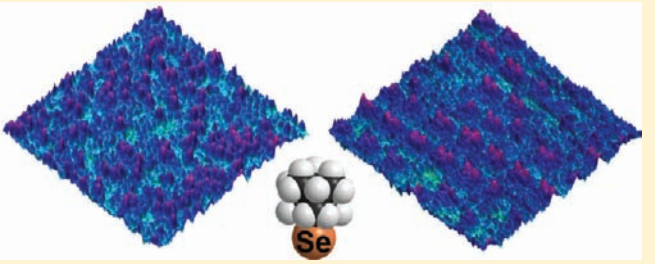

INTRODUCTION

Molecular design can be used to test fundamental assumptions regarding structure and function of supramolecular assemblies. Self-assembled monolayers (SAMs) are a powerful platform to determine how adsorbate geometry, substrate−adsorbate bonds, and interadsorbate forces interact to produce emergent nanoscale structures and macroscale properties.[1−8] After decades of practical application, the nature, chemistry, and structures of the gold−chalcogenate bonds continue to draw interest.[4,9−19] Akin to thiols, selenols bind strongly to gold, producing ordered SAMs on Au{111}.[20−28] There is keen interest in ascertaining the structural and electronic similarities and differences between the Au−Se and Au−S bonds.[29−37] However, studying the Au−Se interface through an *n*-alkaneselenolate monolayer is complicated by the organization of the assembled alkyl tail groups; where *n*-alkanethiolate monolayers display large domains of similarly aligned and tilted molecules,[4] their selenolate analogues show a distinctive moiré pattern of rolling topographical differences, few domain boundaries, and few substrate vacancy island defects.[23] To isolate, to assess, and to understand the gold−selenol attachment structure and chemistry, it is desirable to disentangle geometric and structural variables.

The structure of a SAM is determined primarily by three factors: the molecule/substrate interactions, the shape and packing of the molecules, and the intermolecular interactions. Small geometric alterations can dramatically affect the morphology and properties of emergent, ordered structures.[4,5,38−46] Consider primary *n*-alkanethiols and *n*-alkaneselenols: the molecules assemble differently and display different defect modes, and the attachment atoms are of different sizes.[4,23] An ideal comparison of thiolate and selenolate binding minimizes differences in SAM structure, eliminating the effects of differently organized or oriented molecules. To that end, we have prepared and characterized SAMs of 1-adamantaneselenol (ADSe) on Au{111}, a structural analogue of the extensively characterized 1-adamantanethiolate SAMs on Au{111}.[5,41,42,45,47] In this article, we describe the supramolecular structure and orientation, report dynamic site-dependent conductance switching, and propose a mechanism of substrate mediation that results in an emergent, ordered lattice of aligned rows of high-conductance ADSe dimers.

In our previous work, we have shown that the lattices of thiolates of upright symmetric cage molecules are determined by the projection of the cage on the surface.[5,42,45,46] Thus, these systems, with their simplified defect structures, are well-poised to serve as test structures for comparing headgroup attachment chemistries and other properties.[47−52] The adamantane cage is rigid and symmetric, minimizing the orientational and conformational degrees of freedom of the assembled species. Space-filling models comparing ADSe to the previously investigated 1-adamantanethiol (1AD) are shown in Figure 1.

Received: July 12, 2011
Published: August 23, 2011

dx.doi.org/10.1021/ja2063988 | *J. Am. Chem. Soc.* 2011, 133, 19422–19431

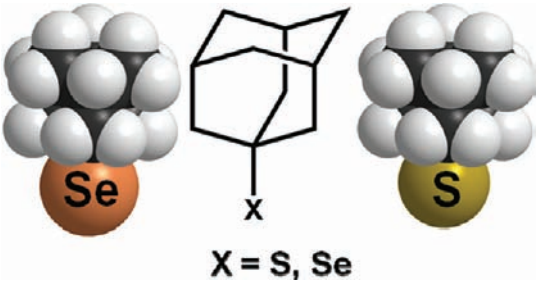

Figure 1. Adamantane diamondoid (center) with space-filling models of 1-adamantaneselenol ($C_{10}H_{15}SeH$, left) and 1-adamantanethiol ($C_{10}H_{15}SH$, right). Despite the larger size of the selenium atom relative to the sulfur, the projection of the adamantane cage remains the determinant geometric factor for the monolayer structure of both compounds.

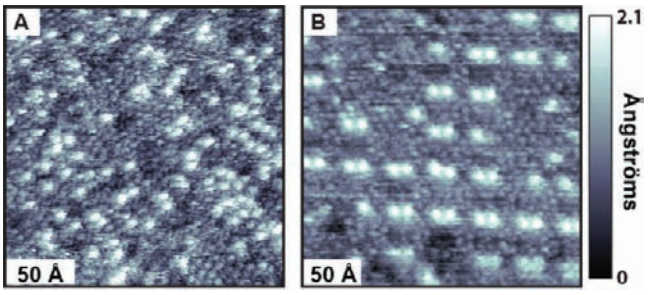

Figure 2. (A) As-deposited and (B) dry-annealed SAMs of 1-adamantaneselenolate on Au{111}. (A) Hexagonally close-packed molecules are distributed randomly between two conductance states. (B) Dry annealing at 70 °C triggers self-organization of the high-conductance molecules into a distinctive dimer structure; low-conductance molecules are not altered appreciably by annealing. Order is long range and persists beyond defects in the dimer-pair lattice (described below). Molecules are dynamic and switch between high- and low-conductance states whether organized or randomly distributed. The 512 × 512 pixel STM images were collected at a sample bias of −1.0 V and 1 pA tunneling current. Image B has been digitally filtered (see the Supporting Information, Figure S1, for the unfiltered image).

RESULTS AND DISCUSSION

Characterization of 1-Adamantaneselenolate Monolayers and Defect Modes. 1-Adamantaneselenol forms a complex overlayer on Au{111}, composed of ADSe in two different binding modes. Figure 2 depicts scanning tunneling microscope (STM) images obtained in air, revealing structural details of as-deposited (from ethanolic solution at room temperature) and dry-annealed (70 °C in air for 18 h) ADSe SAMs (examples are shown in Figure 2). Molecules are deposited from an ethanolic solution and appear in one of two conductance states in STM images. The high-conductance molecules typically comprise 4−8% of the observed molecules before and after annealing. Low-conductance molecules appear hexagonally close-packed, with measured nearest-neighbor spacings of 7.0 ± 0.4 Å, consistent with measurements for 1AD SAMs on Au{111}.[42] High-conductance molecules appear as 1 Å protrusions, and initially appear randomly distributed throughout the lattice. The protrusions also manifest an increase in apparent diameter, because the STM probe senses higher conductance molecules at a greater lateral distance.[53] The measured diameters of such protrusions are dependent on tip shape to some extent. When deposited at room temperature, the two conductance states appear randomly mixed.

Annealing an assembled ADSe film in air at 70 °C drives the self-organization of protruding molecules into a distinctive, long-range ordered structure of aligned molecular pairs (or "dimers"), shown in Figure 2B. As above, high-conductance molecules appear to protrude from the surrounding lattice by 1 Å in STM images with the tunneling conditions shown, but they often appear with larger diameters than their randomly distributed counterparts (which we attribute primarily to a convolving tip and protruding feature structure[54]). There are no systematic differences between the low-conductance molecules before and after annealing, which retain hexagonal close-packing. The ordered domains of similarly aligned dimers can extend to cover entire gold terraces. We define domain directionality as the direction parallel to the aligned molecular pairs. Relative rotations of isolated ordered domains will be described below. The directionality of rows has not been observed to shift smoothly between domains; rotational domain boundaries are separated by disordered regions. Some depressions in the lattice are observed, attributed to pinhole monolayer defects, likely resulting from isolated molecular desorption during annealing. At room temperature, we observe fast conductance switching between the high- and low-conductance modes, regardless of order. For clarity, we will first describe the structural characteristics of both randomly distributed and ordered high-conductance regions, and reserve the discussion of monolayer dynamics until afterward.

The temperature window for ordered dimer emergence is narrow. Annealing up to 60 °C for 24 h revealed no ordered dimer domains, while annealing above 70 °C (typically between 75 and 85 °C) induces partial monolayer desorption, leading to a collapse of the ordered structure. The result of further annealing is the formation of a dynamic structure similar to the missing-row structures observed in *n*-alkaneselenolates.[23] Further discussion of this structure can be found in the Supporting Information.

The random distribution of high-conductance molecules affords little information for the elucidation of the underlying monolayer structure. This assembly is the kinetic SAM product, formed by fast deposition of ADSe at essentially all available binding sites. Importantly, there is no characteristic lattice or repeat structure that links the positions of the low-conductance molecules with the positions of the high-conductance molecules. High-conductance molecules can appear isolated, in pairs, or in groups. Once annealed to the ordered dimer structure, the regularity enables the determination of likely lattice positions for high-conductance molecules. Figure 3 shows representative line scans along and perpendicular to the dimer pairs.

The positions of ordered high-conductance molecules were analyzed to develop a structural model. Image line scans extracted along and perpendicular to the dimers are shown in Figure 3. The measured peak-to-peak separation of dimer pair members (a) is 11.4 ± 1.5 Å. The distances between the first molecules of two pairs and the second molecules of two pairs (b and c, respectively) are equivalent, at 38.9 ± 1.6 Å, and the separation between rows of dimers (d) is 36.9 ± 1.7 Å. Where high-conductance molecules are missing from their expected positions, within ordered domains, the structure resumes after integer multiples of lattice spacings. The regularity of the dimer pair structure, and the tendency for the ordered domains to persist past defect sites with no change in regularity, indicate that

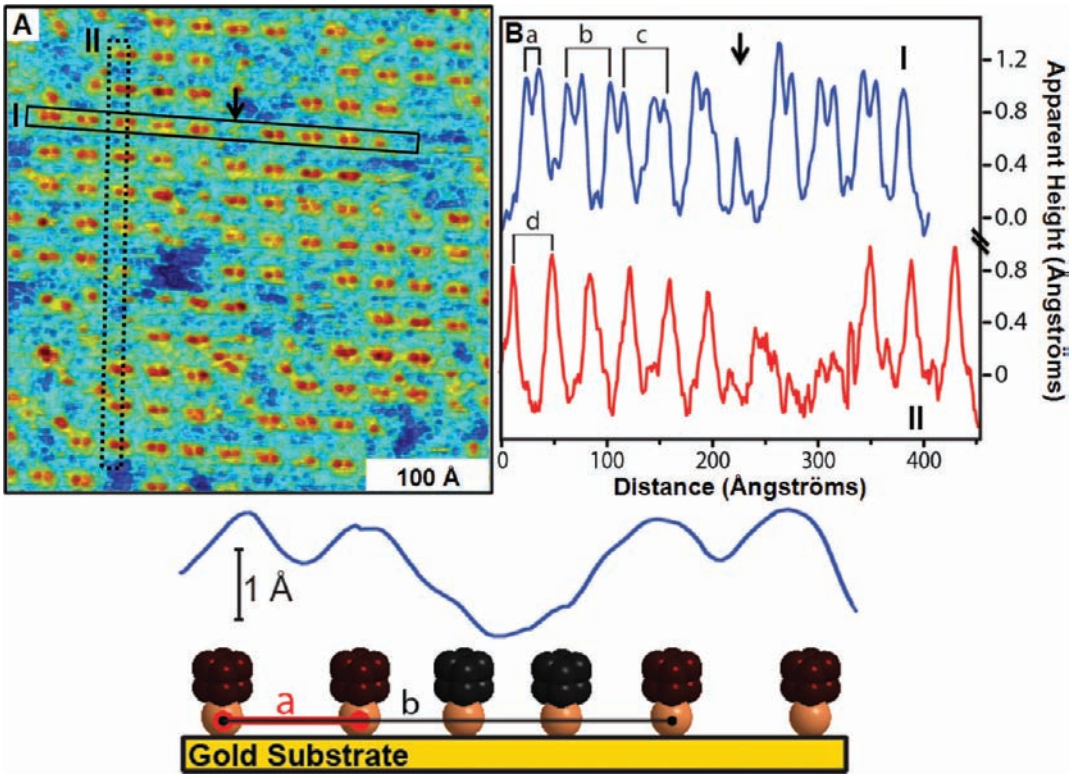

Figure 3. (A) Scanning tunneling microscope (STM) image and (B) line scans of a dry-annealed 1-adamantaneselenolate self-assembled monolayer showing the regularity of distance across pairs (I) and between pairs (II). Separation between paired molecules is 11.4 ± 1.5 Å (a). Separation between the first molecule and second molecule of adjacent pairs is equivalent, at 38.9 ± 1.6 Å (b and c, respectively). Row-to row-distance (d) is 36.9 ± 1.7 Å. Order persists beyond defect sites with no change in regularity; missing-pair and half-pair defects do not affect the regularity of the overall structure, an example noted by the black arrows in panels A and B. (C) Idealized schematic illustration of the contribution of low- and high-conductance molecules to the line scan (blue line) across two dimers. Low-conductance molecules between dimers appear as shoulders on the peaks associated with high-conductance molecules. Distances a and b are noted. High-conductance molecules are tinted red. Image collected at −1 V sample bias and 1 pA tunneling current.

the underlying gold substrate templates and directs the organization of the dimer structure.

Although the annealed ADSe SAMs display high regularity and long-range order, there are characteristic defects that fall into different categories, the most common of which are shown in Figure 4. Each defect described represents a molecule in the alternate conductance state than would be expected, given its position in the ordered lattice. Examples of the ideal dimer structure are shown in Figure 4A. Rarely, a dimer may be separated by a single molecular vacancy; such a pair-gap defect doubles the measured separation of the molecules (Figure 4B). One or both molecules of a dimer may be missing (Figure 4C, D, respectively). Molecules occasionally occupy a central site between two dimer rows and are often slightly closer to one row (Figure 4E). Lastly, some protruding molecules are offset from and do not appear as part of the regular lattice structure (Figure 4F). Defect modes are generally observed in combinations, which can lead to incorrect assignments. For example, a molecule can appear at a characteristic center site (such as Figure 4E) but adjacent to several missing pairs or half-pairs. Such configurations are not unique defect modes and are easily mistaken for offset sites. Importantly, there is an obvious potential defect configuration that is never observed: molecules do not bridge two adjacent pairs, which would manifest as a five-molecule row (nor are linear triplets observed). We will recall this observation below, discussing the structural model for the ordered lattice.

We now address the orientations of the high-conductance dimer rows with respect to the gold lattice and to other ordered rotational domains. Ordered domains often occupy entire gold terraces, which are routinely larger than $(500\ \text{Å})^2$. On suitably large terraces, $(1000\ \text{Å})^2$, multiple domains are observed rotated with respect to one another. Figure 5 depicts a STM image of four discrete domains on a single gold terrace and a fifth domain on a lower terrace. The dimer orientations in each domain are denoted by a colored line. The domains are rotated with respect to one another by integral multiples of 30°. The domain on the lower terrace (black dashed line) matches the orientation of one of the domains on the upper terrace (black line). Taken together, the regular rotational symmetry and the matching of domains on separate gold terraces are additional support for the templating of the dimers by the gold lattice. To determine the approximate rotation of the rows with respect to the underlying gold lattice, the angle between straight step edges and the orientation of rows of dimers are determined. Straight step edges correspond to the close-packed $\langle 1\bar{1}0 \rangle$ direction of the gold atoms, so the angle of rotation for dimer rows with respect to the underlying gold lattice can be determined. As an important aside, we have not observed a change in row directionality within an ordered domain; rotational domains are separated by regions of randomly distributed high-conductance ADSe molecules.

Orientation of Assembled 1-Adamantaneselenolate Monolayers. To determine the orientation of chemisorbed ADSe, we turn to infrared reflectance absorption spectroscopy (IRRAS) of

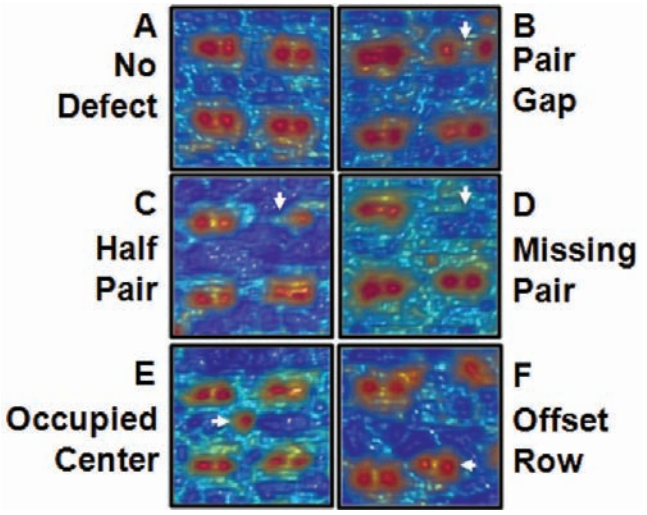

Figure 4. Scanning tunneling microscope images showing commonly observed defect modes of the ordered, annealed 1-adamantaneselenolate SAM on Au{111}. All defects described (denoted by white arrows) represent molecules in the alternate conductance than would be expected given their positions in the lattice. (A) The regular lattice with four high-conductance dimers. (B) Within a row, an offset of one molecule is a pair-gap defect. (C) A lattice position may be missing a single member of a pair, resulting in a half-pair defect, (D) or both molecules, designated a missing pair. (E) Molecules sometimes occupy a central space between four molecular pairs; such occupied centers are sometimes slightly closer to one row by ~1−2 Å. (F) Offset sites are occupied by single molecules or by dimers at uncharacteristic separations and distances, and are generally associated with the edges of ordered domains. Pair-gap and occupied center defect modes map to amply available three-fold hollow sites outside the regular lattice (see Figure 7). Images were collected at −1 V sample bias and 1 pA tunneling current.

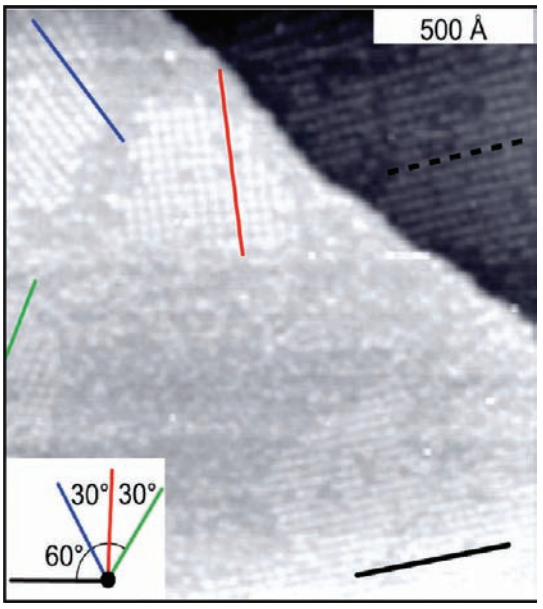

Figure 5. Scanning tunneling microscope image of rows of dimers in a 1-adamantaneselenolate SAM templated by the underlying gold lattice. Domain orientation is defined as parallel to the dimers (refer to Figure 3, line scan I, for reference). The orientations of five ordered domains are denoted by the colored lines. The angles of rotation with respect to one another are integral multiples of 30°. A domain on the lower terrace (dashed black line) has the same lattice orientation as the domain denoted with the black line. The disordered and lower conductance regions separating ordered domains are domains of ADSe with randomly distributed high-conductance molecules. Image were collected at −1 V sample bias and 1 pA tunneling current.

ADSe SAMs. The IR spectra of the ADSe species are shown in Figure 6, before and after deposition. In trace a of Figure 6, the spectrum calculated using density functional theory (DFT) for an isolated ADSe molecule is shown. Apart from some deviations in the signal intensity of CH stretching modes and in the region between 1200 and 1400 cm^{-1}, the predicted spectrum is in good agreement with the spectrum of pure ADSe, which is shown in trace b of Figure 6. Using the calculated results, the bands of the experimental spectra were assigned (in Figure 6b, some of the bands are labeled; see Table S1 in the Supporting Information for their assignments).

The IR spectra of ADSe SAMs deposited from ethanolic solution and from vapor are displayed in traces c and d of Figure 6. Essentially, ADSe SAMs exhibit the same bands as the neat spectrum (b). The bands between 2800 and 3000 cm^{-1} are associated with CH_2 symmetric and asymmetric modes.[42,45,47,55] The negative bands between 1000 and 1100 cm^{-1} correspond to the CD bending modes of the referenced perdeuterated alkanethiolate SAM (additional negative bands corresponding to CD stretching modes between 2000 and 2300 cm^{-1} are not shown). Two bands in the liquid spectrum, at 2299 and 2322 cm^{-1}, are assigned to SeH stretching modes (not shown) and are *not* present in the SAM spectra, consistent with Se−H dissociation upon adsorption.

Band attenuation of IR vibrational modes (specifically, bands labeled 8, 10, and 24 in Figure 6) can be rationalized using the surface selection rule on metal surfaces: vibrational modes whose transition dipole moments (TDMs) are parallel to the substrate surface are extinguished.[56] From the results of the DFT calculations, we have identified that attenuated modes correspond to bands perpendicular to the cage−Se bond of the adamantaneselenol molecule, while those bands that are not attenuated (in particular bands 1, 7, 9, 14, 20, and 25) are parallel to the cage−Se axis.

In an intermediate case, the TDM of band 19 is neither parallel nor perpendicular to the cage−Se axis and displays partial attenuation after SAM deposition. There are some weak bands (12, 15, and 16) that are not markedly attenuated (<30%), despite TDMs nonparallel to the cage−Se axis. However, the spectral data can be best interpreted by assuming that the cage−Se axis is nominally oriented normal to the substrate surface. Qualitatively, the spectrum in Figure 6c is indistinguishable from those of SAMs of 1AD, for which we reached similar conclusions.[42]

Structural Model for ADSe Binding on Au{111}. Recent computational modeling by Scherlis and co-workers[37] predicts that the bridge binding site is the most favorable binding position for selenolates on gold, but demonstrates that both hexagonally close-packed (hcp) and face-centered cubic (fcc) three-fold hollow sites are viable alternative sites,[37] in agreement with our previous report of selenolate−gold bond promiscuity.[23] We have used these predictions and our structural measurements to propose a double lattice model for ordered, annealed ADSe SAMs on Au{111}: one all-bridge configuration for low-conductance molecules, and a three-fold hollow site configuration for high-conductance molecules. Figure 7 depicts a schematic of the lattices for both low-conductance and high-conductance

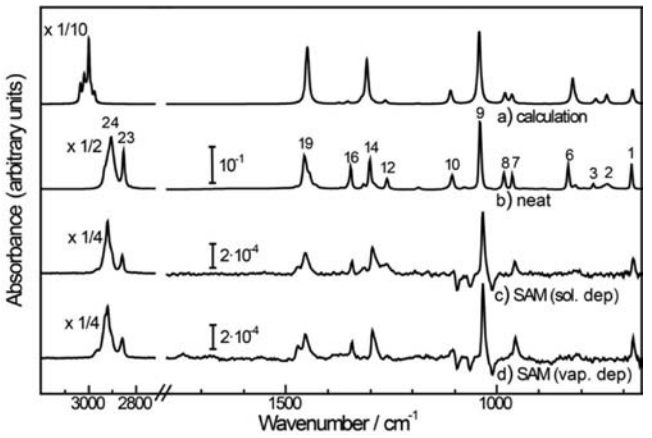

Figure 6. Infrared spectra of ADSe: (a) DFT calculation (B3LYP/cc-pVDZ, energy scaled by a factor of 0.986); (b) spectrum of neat ADSe, recorded with an attenuated total reflection (ATR) unit; (c,d) infrared reflection−absorption spectra (IRRAS) of ADSe SAMs on Au{111}, prepared either by immersion of the substrate into an ethanolic solution of ADSe (c, solution deposited) or by exposing the substrate to the vapor above an ethanolic solution of the selenol (d, vapor deposited). In panel b, some of the vibrational bands are numbered. For details of assignments, see Table S1 in the Supporting Information.

molecules. The low-conductance molecules appear similar in lattice spacing and morphology to the previously measured 1AD monolayer. The previously reported consensus model for 1AD SAMs is the (7×7) lattice in an all-bridge configuration (with equivalent cells rotated by $\pm 21.79°$ with respect to the gold lattice).[41,42,52,57,58] For simplicity, we have modeled the low-conductance ADSe lattice using this (7×7) structure, with a nearest-neighbor spacing of 6.72 Å. There are other structural models that can approximate the 1AD and low-conductance ADSe SAMs, but regardless of the structural model used, we have not identified a configuration that is low-order commensurate with the periodic high-conductance dimer structures.

Overlaid on the low-conductance model are the rows of ordered, high-conductance dimers, shown as red circles in Figure 7. The lower relative coverage of high-conductance molecules is rationalized by the predicted weaker Au−Se bond at three-fold hollow sites relative to bridge sites.[37] We have modeled the structure as a square lattice with equivalent sides of 38.7 Å. This structure can be approximated using a $(6\sqrt{5} \times 6\sqrt{5})R15°$ unit cell. Molecules in rows of dimer pairs occupy alternating fcc and hcp sites on the Au{111} substrate, which correspond to binding configurations that have been linked with higher Au−Se conductance. While there is ample space for an additional molecule between pairs, such a configuration would require occupation of two adjacent fcc or hcp sites. As discussed above, we have not observed a high-conductance defect mode that consists of either three or five aligned molecules. Such a configuration would require the occupation of adjacent fcc or hcp sites, which would break the alternating pattern. We describe the implications of this observation in detail below.

Assuming a fcc unit cell origin for the dimer pair lattice shown in Figure 7, there exist three equivalent and non-superposable dimer orientations rotated with respect to the gold lattice with relative rotations of 120°, as shown in Figure 8. There are three further equivalent non-superposable unit cells that are linked by vertical mirror plane symmetry. For any of these six given unit

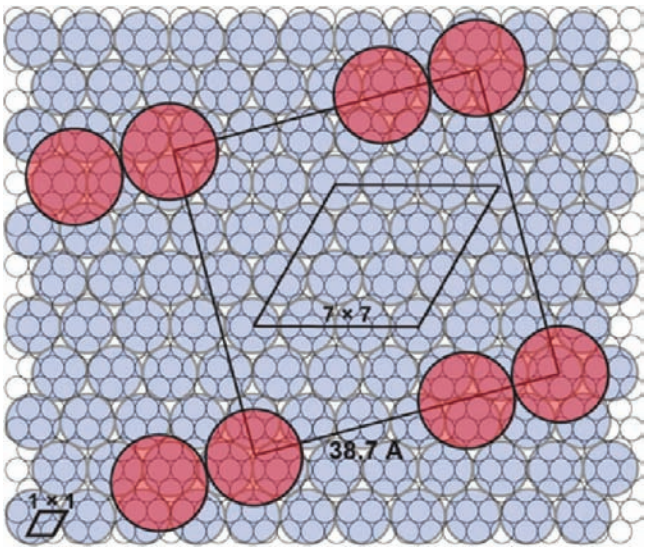

Figure 7. ADSe double lattice on Au{111}, here shown overlaid. A hexagonal lattice for the less protruding ADSe molecules (blue circles) is modeled with a (7×7) unit cell (shown center) on Au{111} (white circles). Molecules in dimer pairs (red circles) appear larger (12.0 Å) and bind at alternating fcc and hcp three-fold hollow sites. The high-conductance unit cell can be described as $(6\sqrt{5} \times 6\sqrt{5})R15°$, with edge lengths of 38.7 Å and 15° rotation with respect to the underlying (1×1) Au{111} lattice. The two unit cells are here shown overlapping, but they compete for (and switch between) binding sites in the monolayer. Importantly, the lattice positions of the low-conductance ADSe molecules do not correspond systematically to the positions of the high-conductance dimers. High-conductance molecule defects that appear outside the regular structure lattice (Figure 4) can be mapped to amply available three-fold hollow sites.

cells with an fcc origin, a corresponding unit cell with hcp origin and matching row orientation will result from taking the vertical and horizontal reflections, as shown in Figure 8. This structural model explains the observed relative dimer orientations: the minor angle between any two rotational domains is always an integral multiple of 30°. There is no physical difference between the unit cells with hcp and fcc origins; we include the notations for completeness of the symmetry discussion.

CONDUCTANCE DYNAMICS

A typical 512×512 pixel image is collected over several minutes. Between observations, molecules switch conductance states at room temperature. Images of domains with random conductance distributions reveal that approximately 2% of observed molecules will switch between subsequent images. The ordered dimer domains appear moderately more stable, with switching events recorded for approximately 1% of observed molecules. Importantly, under normal imaging conditions, the STM observes each molecule for only a few seconds per image, so some of the dynamic events may be missed (at the observed rate, not many); the given percentages are simply illustrative. Artifacts, including streaks and lines, in the image are common indications of dynamics occurring in the presence of the STM tip at time scales faster than that of imaging.[59−64]

Stochastic conductance switching is commonly observed for rigid, conjugated molecules inserted into defect sites of *n*-alkanethiolate SAMs. Such conductance changes are typically attributed to chemical or isomerization reactions,[65−73] or to

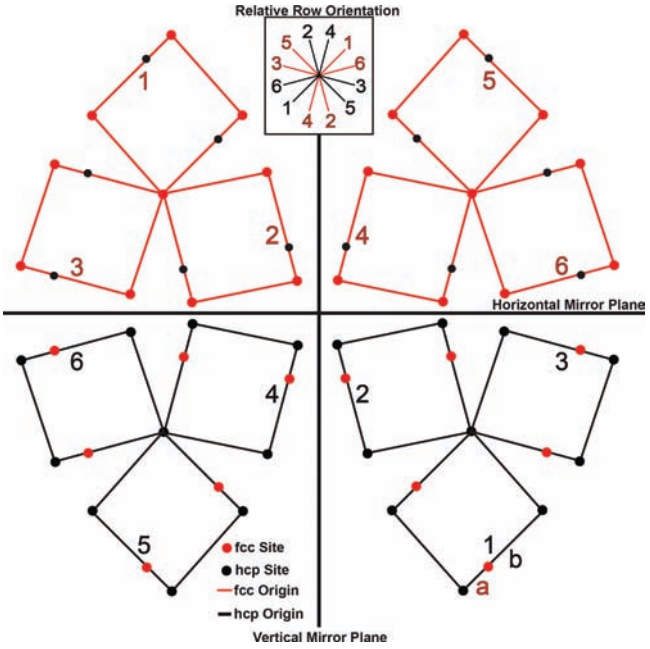

Figure 8. Rotational domains of self-organized high-conductance dimers. Molecules map to alternating fcc (red circles) and hcp (black circles) three-fold hollow sites on Au{111}, and domains are observed rotated with respect to each other in integral multiples of 30°. The red unit cell denoted "1" is rotated in multiples of 120° to give three equivalent, non-superposable unit cells (red: 2, 3). A vertical symmetry axis reveals three additional equivalent, non-superposable unit cells (red: 4, 5, 6). Unit cells centered at fcc sites are linked to hcp-centered unit cells via vertical and horizontal mirror plane symmetry. The legend shows the orientational relationship between the unit cells. The directionality of a cell is taken as parallel to the dimers. The minor angles between any observed dimer direction are always integral multiples of 30°. Distances a and b correspond to the intradimer and unit cell edge lengths of 12.0 and 38.7 Å, respectively.

changes in hybridization of the attachment bond.[65,70,74−82] A recent study of isolated thioethers on Au{111} has linked the dynamics of isolated molecules to the adsorption site.[83] As the adamantane cage is chemically inert under the observation conditions, the observed ADSe conductance changes here are attributed to the attachment chemistry. We note three relevant observations related to switching dynamics. First, switching appears more frequent in regions with lower long-range order; domains with randomly distributed high-conductance molecules tend to be more dynamic (shown in Figure 9), and switching in ordered domains occurs more frequently near defects of the high-conductance lattice (shown in Figure 10). Second, we observe a close match for the on−off and off−on switching rates, resulting in no net change in ratio of molecules in the two states for a given area between observations. Finally, switching is reversible; we have observed an individual position alternating between the two conductance states over a series of images. We have also observed apparent single-site lateral motion of protruding molecules; whether this is true molecular motion or simply two switching events for adjacent molecules has yet to be determined. However, we have not observed long-range lateral motion greater than a single molecular site.

Mechanisms Governing 1-Adamantaneselenolate Self-Assembled Monolayer Structure and Dynamics. We first turn our attention to the mechanism for the appearance of the ordered

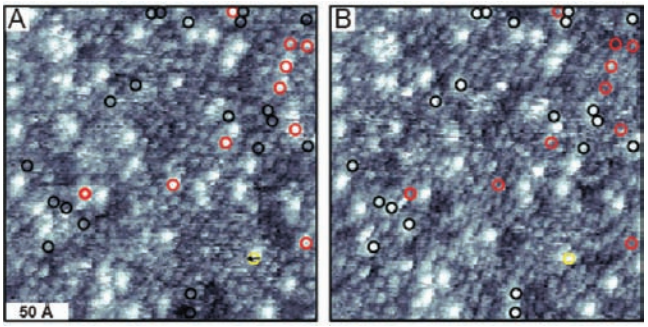

Figure 9. Sequential scanning tunneling microscope images of an unannealed 1-adamantaneselenolate self-assembled monolayer with randomly distributed high-conductance molecules. Molecules switch between low- and high-conductance states faster than the imaging time (minutes). Two sequential images of an as-deposited ADSe film are shown. Molecules with red circles switch to the low-conductance state in the next image, while molecules with black circles have switched to the high-conductance state. The molecule with the yellow circle appears to shift to an adjacent position in the direction of the black arrow. Additional images can be found in the Supporting Information. Images were obtained at a sample bias of −1 V and 1 pA tunneling current.

dimers. The structural model (Figures 7 and 8) for the aligned dimers require high-conductance molecules bound at alternating hcp and fcc sites; we have not observed an ordered configuration that requires adjacent matched sites (hcp adjacent to hcp sites or fcc adjacent to fcc sites). Further, these alternating-site dimers are emergent; kinetically, the random domains dominate, and extended groups of adjacent high-conductance molecules exist (despite being in unfavorable configurations; see Figure 2A). The dynamics at room temperature are insufficient to drive self-organization, but gently annealing the monolayer enables relaxation into the (presumably more thermodynamically stable) ordered domains.

Recall that the high-conductance molecules comprise only a fraction of the total molecules in the monolayer; the question, then, is what directs the self-organization of ADSe molecules separated both by distances greater than 2 nm and by molecules occupying bridge sites? Assembled molecules are well-known to interact in chains over long distances by their aggregate intermolecular forces,[5,46,65,84−93] but the only direct intermolecular interactions present within an ADSe SAM are weak van der Waals interactions between adjacent adamantane cages.[42,45] If interactions between molecules are not responsible for the emergence of long-range order, then that order must originate from the substrate.[94−97] We postulate that substrate mediation of selenium binding sites is directing the appearance of the dimer pairs; a molecule at one site is altering the substrate electronic structure, thus modifying the affinity for and stability of ADSe adsorption at nearby sites. Empirically, the interaction of an ADSe molecule at a hcp site makes attachment at adjacent hcp sites less favorable, but binding at an adjacent fcc site more favorable, creating a dimer. The dimers can then cooperatively exert their influence at long range, resulting in the observed uniform rows. We note that the long noble metal Fermi wavelength for Au{111}, approximately 37.6 Å,[98−100] is close to the observed unit cell repeat of 38.7 Å. Further investigations into the selenolate−gold interaction and the underlying electronic structure are warranted.

Monolayer dynamics provide a chemical path from one configuration to the next. Our structural model is site-dependent: we

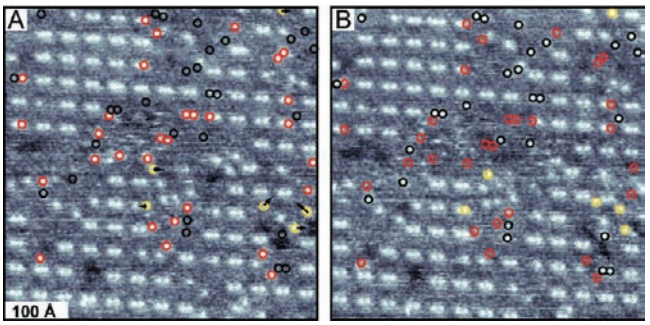

Figure 10. Two sequential scanning tunneling microscope images of an annealed 1-adamantaneselenolate self-assembled monolayer in which high-conductance dimers are ordered. Molecules switch between low- and high-conductance states between images. There is a preference, but not a restriction, for dynamics at or adjacent to defect sites and in regions of disorder. Molecules with red circles switch to the low-conductance state in the subsequent image, while molecules with black circles have just switched to the high-conductance state in the image shown. Molecules bounded by the yellow circles appear to have moved to adjacent lattice positions, but may be due to two molecules in adjacent positions switching separately. Images were obtained at a sample bias of −1 V and 1 pA tunneling current. See the Supporting Information for the unannotated images.

presume that molecules hop between bridge and three-fold hollow sites, an event that results in the apparent conductance switching.[37] Further, this site-hopping provides a mechanism for reaching the favorable, ordered configuration. Molecules switch more frequently at (or near) defects of the ordered dimers. Once incorporated into the emerging ordered domains, the switching rate decreases, which leads eventually to the long-range ordered film. More frequent switching at defect sites relative to ordered sites will favor the extension of the ordered regions. Elevated temperatures presumably increase the dynamic rate, surface mobility, and tendency to create pinhole defects in the monolayer by molecular desorption; all of these effects combine to favor the self-organization process that leads to the ordered regions. We note that a potentially critical enabling factor of ADSe monolayer dynamics is the low intermolecular interactions present between molecules.

■ CONCLUSIONS AND PROSPECTS

1-Adamantaneselenolate SAMs adopt a dynamic double lattice on Au{111}. Molecules assume high- and low-conductance modes and switch stochastically between the two states, a property enabled by the low energetic barrier to motion of assembled adamantane cages. STM images of ADSe SAMs deposited at room temperature reveal that the two states are mixed randomly, but gently annealing the sample at 70 °C induces self-organization of the high-conductance molecules into aligned rows of molecular pairs. Infrared measurements show that the molecules stand upright, with the cage−Se axis nominally normal to the surface. We modeled the low-conductance mode with a (7×7) lattice in an all-bridge configuration, which is structurally similar to the analogous 1AD monolayer on gold. The ordered pair structure is less dynamic than the random distribution, suggesting that selenols in alternating hcp and fcc sites constitute a preferred configuration. We conclude that the dynamics of the molecules eventually results in the emergence of the ordered structure, driven by substrate mediation acting especially at three-fold hollow sites. Our models provide a mechanism for describing both the emergence of the ordered dimer structure and how the transition to order occurs.

For the comparison of aliphatic thiols to selenols, merely ranking thiolate and selenolate conductivity is not straightforward. We have previously described the effects of band alignment, which is dependent on both the attachment chemistry and the molecular backbone.[34,101] The observation of well-defined, dynamic site-dependent conductance states for selenolate assemblies is an important design detail to consider when developing molecular electronic devices based on selenolate−gold chemistry.[33,102,103] The models for structure and dynamics we described will be tested in part with further iterations of molecular design. Increasing or decreasing the molecular size and incorporating interactions between functional groups will reveal further details of the nature of selenolate-based attachments for monolayers.

The relative abundance of high-conductance molecules at three-fold hollow sites and low-conductance molecules at bridge sites is in agreement with theoretical predictions.[37] However, it is not clear *why* a molecule bound at a hollow site should be more conductive than a molecule at a bridge site; the opposite trend for thiolates has been predicted and reported in break junction devices.[104,105] We assume a simple binding motif of the selenium atom resting in its binding site. This assumption was also made early in the study of alkanethiolates on gold and was later called into question. There is continuing scientific debate regarding the interpretation of results for the atomistic nature of the Au−S bond, especially with regard to the binding site (bridge, three-fold hollow, or atop), and the effect of gold adatoms on the lifting of the gold herringbone reconstruction and in the final monolayer.[11,15−18,30,106−112] There has been little complementary work on the structure of the Au−Se bond. The geometric simplicity and well-defined structure of ADSe SAMs on Au{111} make the system an ideal target for experimental observation and for the computational modeling of selenolate-based monolayers. The adamantane cage eliminates the intrinsic complexity (tilt, conformational degrees of freedom) of *n*-alkaneselenol assemblies: the adamantane is rigid, stands normal to the surface, interacts only weakly with neighbors, and predominantly displays two distinct binding types. There is rich opportunity for a confluence of molecular design, experimental analysis, and theoretical treatment to lead to the development of a general motif for chalcogenate binding.

■ EXPERIMENTAL METHODS

Synthesis of the Adamantaneselenol. To a suspension of fine magnesium turnings (17.89 g, 726.2 mmol) in absolute ether (400 mL) were added 1-bromoadamantane (10.78 g, 50.11 mmol) and 1,2-dibromoethane (0.2 mL). The mixture was heated to reflux for 16 h, after which the Grignard solution was retrieved from the remaining Mg using a syringe. When this solution was added to gray selenium (4.69 g, 59.4 mmol), no discernible reaction took place, but the mixture became warm upon addition of tetrahydrofuran (THF, 100 mL). After 20 h of stirring at room temperature, the reaction was quenched by addition of water and stirred for 1 h with air contact. The organic phase was separated, the aqueous phase extracted with ether, and the combined organic phases evaporated to dryness. The residual solid was taken up in dichloromethane, washed with water, and evaporated again. The solid was purified by train sublimation in high vacuum at 200 °C, yielding a yellow-orange solid, which was identified by ^{77}Se NMR spectroscopy as a mixture of diselenide and triselenide. This intermediate was dissolved

in absolute THF (20 mL) and reduced by addition of $LiAlH_4$ (0.5 g) while stirring for 24 h at room temperature. The mixture was quenched by addition of dilute HCl (40 mL, 20%). The product was extraced twice with deaerated chloroform, followed by removal of the solvent and distillation *in vacuo*, yielding 2.26 g (10.5 mmol) of a colorless, air-sensitive oil (21%).

^{1}H NMR ($CDCl_3$, 300 MHz): δ = 2.11 (d, 6H, ^3J = 3.0 Hz, C**H**$_2$), 1.98 (ms, 3H, C**H**), 1.72−1.67 (m, 6H, C**H**$_2$), 0.05 (s, 1H, Se**H**) ppm.

^{13}C NMR ($CDCl_3$, 75 MHz): δ = 48.6 (**C**H$_2$), 43.8 (**C**SeH), 35.8 (**C**H$_2$), 30.9 (**C**H) ppm.

^{77}Se NMR ($CDCl_3$, 57 MHz): δ = 269.6 (d, ^1J = 46.0 Hz) ppm.

MS (EI): *m*/*z*= 135 (100%, Ada$^+$), 216 (1%, M$^+$).

Elemental analysis: $C_{10}H_{16}Se$ (215.19), calculated (%) C 55.81, H, 7.49; found C 54.96, H 7.30.

Monolayer Preparation. 1-Adamantaneselenolate monolayers for STM imaging were deposited from oxygen-free 1 μL/mL ethanolic solution onto commercially available Au/mica substrates (Agilent, Santa Clara, CA). Ethanol (undenatured, 200 proof, Sigma-Aldrich, St. Louis, MO) was degassed by six freeze−pump−thaw cycles in an air-free flask (Chemglass, part no. AF-0522, Vineland, NJ). The ethanol-rinsed flask was stored in a 100 °C drying oven until use. It was loaded with 125 mL of freshly opened ethanol. Each cycle began with freezing the ethanol solid in a liquid nitrogen bath. The flask was then mechanically evacuated at 10^{-3} Torr. The flask was resealed and placed in a lukewarm water bath to thaw, taking care to avoid agitation. After six cycles, the sealed flask was transferred to a glovebox with an internal oxygen content of <1 ppm. 1-Adamantaneselenol was stored inside the glovebox environment, and solutions were typically prepared immediately before use. We made every effort to minimize the time between substrate preparation and immersion. The Au/mica substrates were annealed with 40 passes of a hydrogen flame (at a rate of 0.5 Hz), sealed into a gasketed plastic vial (National Scientific, part no. BS20NA-BP, Claremont, CA), and then quickly transferred to the glovebox. Once transferred, the vial was opened and the sample placed in the ADSe solution, minimizing substrate exposure to the glovebox environment. The sample solution was then capped.

After 24 h of assembly, the sample was removed from the ADSe solution and placed in a vial of neat ethanol. This secondary vial was then removed from the glovebox, at which time the sample was rinsed three times with ethanol and dried with a stream of nitrogen gas. Samples could then be imaged, or were sealed in an empty glass v-vial and held at the appropriate temperature for 18 h of dry annealing.[45] Dry annealing is defined as heating the sample in the absence of solution at a set elevated temperature. We use rampless heating, placing the sample into the preheated chamber of a Barnstead Thermolyne 1400 furnace (ThermoFisher Scientific, Waltham, MA). It is important that the furnace maintains the target temperature within 1 °C throughout the annealing process, as the temperature window for ADSe self-organization is narrow, and film desorption begins to occur above 75 °C. After dry annealing, samples were rinsed with ethanol three additional times and dried with a stream of nitrogen.

Sample Preparation for IR Measurements. Gold substrates were prepared by subsequent thermal evaporation of 5 nm of titanium and 200 nm of gold (99.99% purity) onto polished single-crystal Si(100) wafers. To clean the substrates, they were rinsed with ethanol and immersed for about 30 min into an ethanolic solution of 1-octadecanethiol, followed by 2 min treatment in a H_2 plasma.

Self-assembled monolayers were prepared in two different manners: (1) By 22 h immersion of the substrate into a ∼0.2 mM solution of ADSe in ethanol at room temperature. After removal from the solution, the sample was rinsed carefully with ethanol and dried with gaseous nitrogen. (2) By exposure of a substrate to the vapor above a ∼0.2 mM solution of adamantaneselenol in ethanol for ∼18 h at 70 °C. This sample was used without any further treatment.

Scanning Tunneling Microscopy. All STM measurements were performed in air using a custom beetle-style STM and a platinum/iridium tip (80:20).[113,114] The well-known lattice of the 1-dodecanethiolate SAMs on Au{111} was used to calibrate piezoelectric scanners,[115] and these calibrations were subsequently checked against the expected spacings of a 1AD SAM.[42] Unless otherwise specified, the sample was held at −1 V bias, and 512 × 512 pixel images were collected in constant-current mode with a tunneling current of 1 pA. We note strong tip dependence for imaging cage molecules.

Infrared Spectroscopy. Infrared spectra were measured with a Thermo Nicolet 6700 Fourier Transform IR spectrometer (ThermoFisher Scientific) equipped with a liquid-nitrogen-cooled narrow-band mercury cadmium telluride detector. The complete beam path of the spectrometer was purged with dried and CO_2-free air. Spectra of neat ADSe were obtained using a diamond ATR unit. Infrared spectra of the ADSe SAMs were recorded at grazing incidence (80° relative to the sample surface normal). Reference spectra were taken from SAMs of perdeuterated hexadecanethiolate on Au(111). All spectra were acquired at a resolution of 4 cm^{-1}.

Density Functional Theory Calculations. The vibrational spectrum of 1-adamantaneselenol was calculated with DFT methods using the Gaussian 09 program package.[116] We performed calculations using two different DFT functionals (B3LYP, BP86) and a range of basis sets (6-31++G(d,p), SVP, cc-pVDZ). The results were used to aid the assignment of the vibrational bands of the ADSe spectrum and to estimate the directions of the corresponding TDMs. The result of the B3LYP/cc-pVDZ DFT calculation turned out to be in accord with the experimental spectra and thus was further used for band assignment and identification of the direction of their TDMs.

■ ASSOCIATED CONTENT

Supporting Information. Scanning tunneling microscope images of 1-adamanataneselenolate SAMs annealed at 70 and 85 °C; discussion of the structure and dynamics of partially desorbed monolayers; additional details and images of monolayer dynamics for annealed and unannealed SAMs; complete ref 116. This material is available free of charge via the Internet at http://pubs.acs.org.

■ AUTHOR INFORMATION

Corresponding Author
aterfort@chemie.uni-frankfurt.de; psw@cnsi.ucla.edu

■ ACKNOWLEDGMENT

The authors thank Drs. Shelley Claridge and Mitchell Shuster for their invaluable discussions and editing, and Mr. David McMillan for technical support. J.N.H. thanks the Applied Research Lab (ONR) for a graduate fellowship. This work was supported by the National Science Foundation and the Kavli Foundation.

■ REFERENCES

(1) Nuzzo, R. G.; Allara, D. L. *J. Am. Chem. Soc.* **1983**, *105*, 4481–4483.
(2) Bain, C. D.; Whitesides, G. M. *Science* **1988**, *240*, 62–63.
(3) Kumar, A.; Biebuyck, H. A.; Whitesides, G. M. *Langmuir* **1994**, *10*, 1498–1511.
(4) Love, J. C.; Estroff, L. A.; Kriebel, J. K.; Nuzzo, R. G.; Whitesides, G. M. *Chem. Rev.* **2005**, *105*, 1103–1169.
(5) Hohman, J. N.; Claridge, S. A.; Kim, M.; Weiss, P. S. *Mater. Sci. Eng., R* **2010**, *70*, 188–208.

(6) Saavedra, H. M.; Mullen, T. J.; Zhang, P. P.; Dewey, D. C.; Claridge, S. A.; Weiss, P. S. *Rep. Prog. Phys.* **2010**, *73*, 036501.
(7) Heimel, G.; Rissner, F.; Zojer, E. *Adv. Mater.* **2010**, *22*, 2494–2513.
(8) Smith, R. K.; Lewis, P. A.; Weiss, P. S. *Prog. Surf. Sci.* **2004**, *75*, 1–68.
(9) Maksymovych, P.; Sorescu, D. C.; Yates, J. T. *Phys. Rev. Lett.* **2006**, *97*, 146103.
(10) Mazzarello, R.; Cossaro, A.; Verdini, A.; Rousseau, R.; Casalis, L.; Danisman, M. F.; Floreano, L.; Scandolo, S.; Morgante, A.; Scoles, G. *Phys. Rev. Lett.* **2007**, *98*, 4.
(11) Woodruff, D. P. *Phys. Chem. Chem. Phys.* **2008**, *10*, 7211–7221.
(12) Ariga, K.; Hill, J. P.; Lee, M. V.; Vinu, A.; Charvet, R.; Acharya, S. *Sci. Technol. Adv. Mater.* **2008**, *9*, 014109.
(13) Gronbeck, H.; Hakkinen, H.; Whetten, R. L. *J. Phys. Chem. C* **2008**, *112*, 15940–15942.
(14) Lopez-Acevedo, O.; Akola, J.; Whetten, R. L.; Gronbeck, H.; Hakkinen, H. *J. Phys. Chem. C* **2009**, *113*, 5035–5038.
(15) Torres, E.; Blumenau, A. T.; Biedermann, P. U. *Phys. Rev. B* **2009**, *79*, 075440.
(16) Franke, A.; Pehlke, E. *Phys. Rev. B* **2009**, *79*, 235441.
(17) Han, P.; Kurland, A. R.; Giordano, A. N.; Nanayakkara, S. U.; Blake, M. M.; Pochas, C. M.; Weiss, P. S. *ACS Nano* **2009**, *3*, 3115–3121.
(18) Maksymovych, P.; Voznyy, O.; Dougherty, D. B.; Sorescu, D. C.; Yates, J. T. *Prog. Surf. Sci.* **2010**, *85*, 206–240.
(19) Tsuji, Y.; Staykov, A.; Yoshizawa, K. *J. Am. Chem. Soc.* **2011**, *133*, 5955–5965.
(20) Samant, M. G.; Brown, C. A.; Gordon, J. G. *Langmuir* **1992**, *8*, 1615–1618.
(21) Dishner, M. H.; Hemminger, J. C.; Feher, F. J. *Langmuir* **1997**, *13*, 4788–4790.
(22) Yee, C. K.; Ulman, A.; Ruiz, J. D.; Parikh, A.; White, H.; Rafailovich, M. *Langmuir* **2003**, *19*, 9450–9458.
(23) Monnell, J. D.; Stapleton, J. J.; Jackiw, J. J.; Dunbar, T.; Reinerth, W. A.; Dirk, S. M.; Tour, J. M.; Allara, D. L.; Weiss, P. S. *J. Phys. Chem. B* **2004**, *108*, 9834–9841.
(24) Banica, A.; Culetu, A.; Banica, F. G. *J. Electroanal. Chem.* **2007**, *599*, 100–110.
(25) Bashir, A.; Käfer, D.; Müller, J.; Wöll, C.; Terfort, A.; Witte, G. *Angew. Chem., Int. Ed.* **2008**, *47*, 5250–5252.
(26) Cyganik, P.; Szelagowska-Kunstman, K.; Terfort, A.; Zharnikov, M. *J. Phys. Chem. C* **2008**, *112*, 15466–15473.
(27) Choi, J.; Lee, Y. J.; Kang, H.; Han, J. W.; Noh, J. *Bull. Korean Chem. Soc.* **2008**, *29*, 1229–1232.
(28) Weidner, T.; Ballav, N.; Grunze, M.; Terfort, A.; Zharnikov, M. *Phys. Status Solidi B* **2009**, *246*, 1519–1528.
(29) Yaliraki, S. N.; Kemp, M.; Ratner, M. A. *J. Am. Chem. Soc.* **1999**, *121*, 3428–3434.
(30) Yu, M.; Bovet, N.; Satterley, C. J.; Bengio, S.; Lovelock, K. R. J.; Milligan, P. K.; Jones, R. G.; Woodruff, D. P.; Dhanak, V. *Phys. Rev. Lett.* **2006**, *97*, 166102.
(31) Di Ventra, M.; Lang, N. D. *Phys. Rev. B* **2001**, *65*, 045402.
(32) Protsailo, L. V.; Fawcett, W. R.; Russell, D.; Meyer, R. L. *Langmuir* **2002**, *18*, 9342–9349.
(33) Patrone, L.; Palacin, S.; Bourgoin, J. P. *Appl. Surf. Sci.* **2003**, *212*, 446–451.
(34) Monnell, J. D.; Stapleton, J. J.; Dirk, S. M.; Reinerth, W. A.; Tour, J. M.; Allara, D. L.; Weiss, P. S. *J. Phys. Chem. B* **2005**, *109*, 20343–20349.
(35) Heimel, G.; Romaner, L.; Zojer, E.; Bredas, J. L. *Nano Lett.* **2007**, *7*, 932–940.
(36) Yokota, K.; Taniguchi, M.; Kawai, T. *J. Am. Chem. Soc.* **2007**, *129*, 5818–5819.
(37) de la Llave, E.; Scherlis, D. A. *Langmuir* **2010**, *26*, 173–178.
(38) Walczak, M. M.; Chung, C. K.; Stole, S. M.; Widrig, C. A.; Porter, M. D. *J. Am. Chem. Soc.* **1991**, *113*, 2370–2378.
(39) Fujii, S.; Akiba, U.; Fujihira, M. *Chem. Commun.* **2001**, *2001*, 1688–1689.
(40) Han, S. W.; Lee, S. J.; Kim, K. *Langmuir* **2001**, *17*, 6981–6987.
(41) Fujii, S.; Akiba, U.; Fujihira, M. *J. Am. Chem. Soc.* **2002**, *124*, 13629–13635.
(42) Dameron, A. A.; Charles, L. F.; Weiss, P. S. *J. Am. Chem. Soc.* **2005**, *127*, 8697–8704.
(43) Base, T.; Bastl, Z.; Plzak, Z.; Grygar, T.; Plesek, J.; Carr, M. J.; Malina, V.; Subrt, J.; Bohacek, J.; Vecernikova, E.; Kriz, O. *Langmuir* **2005**, *21*, 7776–7785.
(44) Heimel, G.; Romaner, L.; Bredas, J. L.; Zojer, E. *Langmuir* **2008**, *24*, 474–482.
(45) Kim, M.; Hohman, J. N.; Morin, E. I.; Daniel, T. A.; Weiss, P. S. *J. Phys. Chem. A* **2009**, *113*, 3895–3903.
(46) Hohman, J. N.; Zhang, P. P.; Morin, E. I.; Han, P.; Kim, M.; Kurland, A. R.; McClanahan, P. D.; Balema, V. P.; Weiss, P. S. *ACS Nano* **2009**, *3*, 527–536.
(47) Saavedra, H. M.; Barbu, C. M.; Dameron, A. A.; Mullen, T. J.; Crespi, V. H.; Weiss, P. S. *J. Am. Chem. Soc.* **2007**, *129*, 10741–10746.
(48) Fujii, S.; Akiba, U.; Fujihira, M. *Appl. Surf. Sci.* **2003**, *210*, 79–83.
(49) Dameron, A. A.; Hampton, J. R.; Gillmor, S. D.; Hohman, J. N.; Weiss, P. S. *J. Vac. Sci. Technol., B* **2005**, *23*, 2929–2932.
(50) Dameron, A. A.; Hampton, J. R.; Smith, R. K.; Mullen, T. J.; Gillmor, S. D.; Weiss, P. S. *Nano Lett.* **2005**, *5*, 1834–1837.
(51) Dameron, A. A.; Mullen, T. J.; Hengstebeck, R. W.; Saavedra, H. M.; Weiss, P. S. *J. Phys. Chem. C* **2007**, *111*, 6747–6752.
(52) Willey, T. M.; Fabbri, J. D.; Lee, J. R. I.; Schreiner, P. R.; Fokin, A. A.; Tkachenko, B. A.; Fokina, N. A.; Dahl, J. E. P.; Carlson, R. M. K.; Vance, A. L.; Yang, W. L.; Terminello, L. J.; van Buuren, T.; Melosh, N. A. *J. Am. Chem. Soc.* **2008**, *130*, 10536–10544.
(53) Weiss, P. S.; Eigler, D. M. *Phys. Rev. Lett.* **1993**, *71*, 3139–3142.
(54) Cygan, M. T.; Dunbar, T. D.; Arnold, J. J.; Bumm, L. A.; Shedlock, N. F.; Burgin, T. P.; Jones, L.; Allara, D. L.; Tour, J. M.; Weiss, P. S. *J. Am. Chem. Soc.* **1998**, *120*, 2721–2732.
(55) Jensen, J. O. *Spectrochim. Acta, Part A* **2004**, *60*, 1895–1905.
(56) Born, M.; Wolf, E. *Principles of Optics*, 2nd ed.; Cambridge University Press: Cambridge, 1999.
(57) Zhou, J. H.; Zhu, R. X.; Shi, L. W.; Zhang, T.; Chen, M. B. *Chin. J. Chem.* **2007**, *25*, 1474–1479.
(58) Azzam, W.; Bashir, A.; Shekhah, O. *Appl. Surf. Sci.* **2011**, *257*, 3739–3747.
(59) Binnig, G.; Fuchs, H.; Stoll, E. *Surf. Sci. Lett.* **1986**, *169*, L295–L300.
(60) Stranick, S. J.; Kamna, M. M.; Weiss, P. S. *Science* **1994**, *266*, 99–102.
(61) Bohringer, M.; Schneider, W. D.; Berndt, R.; Glockler, K.; Sokolowski, M.; Umbach, E. *Phys. Rev. B* **1998**, *57*, 4081–4087.
(62) Berner, S.; Brunner, M.; Ramoino, L.; Suzuki, H.; Guntherodt, H. J.; Jung, T. A. *Chem. Phys. Lett.* **2001**, *348*, 175–181.
(63) Sykes, E. C. H.; Han, P.; Weiss, P. S. *J. Phys. Chem. B* **2003**, *107*, 5016–5021.
(64) Han, P.; Mantooth, B. A.; Sykes, E. C. H.; Donhauser, Z. J.; Weiss, P. S. *J. Am. Chem. Soc.* **2004**, *126*, 10787–10793.
(65) Lewis, P. A.; Inman, C. E.; Yao, Y. X.; Tour, J. M.; Hutchison, J. E.; Weiss, P. S. *J. Am. Chem. Soc.* **2004**, *126*, 12214–12215.
(66) Sullivan, S. P.; Schmeders, A.; Mbugua, S. K.; Beebe, T. P. *Langmuir* **2005**, *21*, 1322–1327.
(67) Zareie, M. H.; Barber, J.; McDonagh, A. M. *J. Phys. Chem. B* **2006**, *110*, 15951–15954.
(68) Iancu, V.; Hla, S. W. *Proc. Natl. Acad. Sci. U.S.A.* **2006**, *103*, 13718–13721.
(69) Kumar, A. S.; Ye, T.; Takami, T.; Yu, B. C.; Flatt, A. K.; Tour, J. M.; Weiss, P. S. *Nano Lett.* **2008**, *8*, 1644–1648.
(70) Weiss, P. S. *Acc. Chem. Res.* **2008**, *41*, 1772–1781.
(71) van der Molen, S. J.; Liao, J. H.; Kudernac, T.; Agustsson, J. S.; Bernard, L.; Calame, M.; van Wees, B. J.; Feringa, B. L.; Schonenberger, C. *Nano Lett.* **2009**, *9*, 76–80.
(72) Molen, S. J. v. d.; Peter, L. *J. Phys.: Condens. Matter* **2010**, *22*, 133001.
(73) Kim, M.; Hohman, J. N.; Cao, Y.; Houk, K. N.; Ma, H.; Jen, A. K.-Y.; Weiss, P. S. *Science* **2011**, *331*, 1312–1315.

(74) Donhauser, Z. J.; Mantooth, B. A.; Kelly, K. F.; Bumm, L. A.; Monnell, J. D.; Stapleton, J. J.; Price, D. W.; Rawlett, A. M.; Allara, D. L.; Tour, J. M.; Weiss, P. S. *Science* **2001**, *292*, 2303–2307.
(75) Wakamatsu, S.; Fujii, S.; Akiba, U.; Fujihira, M. *Nanotechnology* **2003**, *14*, 258–263.
(76) Wang, K.; Zhang, C.; Loy, M. M. T.; Xiao, X. *Phys. Rev. Lett.* **2005**, *94*, 036103.
(77) Moore, A. M.; Mantooth, B. A.; Donhauser, Z. J.; Maya, F.; Price, D. W.; Yao, Y. X.; Tour, J. M.; Weiss, P. S. *Nano Lett.* **2005**, *5*, 2292–2297.
(78) Moore, A. M.; Dameron, A. A.; Mantooth, B. A.; Smith, R. K.; Fuchs, D. J.; Ciszek, J. W.; Maya, F.; Yao, Y. X.; Tour, J. M.; Weiss, P. S. *J. Am. Chem. Soc.* **2006**, *128*, 1959–1967.
(79) Harikumar, K. R.; Polanyi, J. C.; Sloan, P. A.; Ayissi, S.; Hofer, W. A. *J. Am. Chem. Soc.* **2006**, *128*, 16791–16797.
(80) Moore, A. M.; Mantooth, B. A.; Donhauser, Z. J.; Yao, Y. X.; Tour, J. M.; Weiss, P. S. *J. Am. Chem. Soc.* **2007**, *129*, 10352–10353.
(81) Saedi, A.; Poelsema, B.; Zandvliet, H. J. W. *Phys. Rev. B* **2009**, *79*, 153402.
(82) Moore, A. M.; Yeganeh, S.; Yao, Y. X.; Claridge, S. A.; Tour, J. M.; Ratner, M. A.; Weiss, P. S. *ACS Nano* **2010**, *4*, 7630–7636.
(83) Tierney, H. L.; Jewell, A. D.; Baber, A. E.; Iski, E. V.; Sykes, E. C. H. *Langmuir* **2010**, *26*, 15350–15355.
(84) Sprik, M.; Delamarche, E.; Michel, B.; Rothlisberger, U.; Klein, M. L.; Wolf, H.; Ringsdorf, H. *Langmuir* **1994**, *10*, 4116–4130.
(85) Tam-Chang, S.-W.; Biebuyck, H. A.; Whitesides, G. M.; Jeon, N.; Nuzzo, R. G. *Langmuir* **1995**, *11*, 4371–4382.
(86) Takami, T.; Delamarche, E.; Michel, B.; Gerber, C.; Wolf, H.; Ringsdorf, H. *Langmuir* **1995**, *11*, 3876–3881.
(87) Clegg, R. S.; Hutchison, J. E. *Langmuir* **1996**, *12*, 5239–5243.
(88) Dannenberger, O.; Weiss, K.; Himmel, H. J.; Jager, B.; Buck, M.; Woll, C. *Thin Solid Films* **1997**, *307*, 183–191.
(89) Clegg, R. S.; Reed, S. M.; Hutchison, J. E. *J. Am. Chem. Soc.* **1998**, *120*, 2486–2487.
(90) Himmel, H. J.; Terfort, A.; Woll, C. *J. Am. Chem. Soc.* **1998**, *120*, 12069–12074.
(91) Lewis, P. A.; Smith, R. K.; Kelly, K. F.; Bumm, L. A.; Reed, S. M.; Clegg, R. S.; Gunderson, J. D.; Hutchison, J. E.; Weiss, P. S. *J. Phys. Chem. B* **2001**, *105*, 10630–10636.
(92) Smith, R. K.; Reed, S. M.; Lewis, P. A.; Monnell, J. D.; Clegg, R. S.; Kelly, K. F.; Bumm, L. A.; Hutchison, J. E.; Weiss, P. S. *J. Phys. Chem. B* **2001**, *105*, 1119–1122.
(93) Kim, M.; Hohman, J. N.; Serino, A. C.; Weiss, P. S. *J. Phys. Chem. C* **2010**, *114*, 19744–19751.
(94) Sykes, E. C. H.; Mantooth, B. A.; Han, P.; Donhauser, Z. J.; Weiss, P. S. *J. Am. Chem. Soc.* **2005**, *127*, 7255–7260.
(95) Forster, F.; Bendounan, A.; Ziroff, J.; Reinert, F. *Phys. Rev. B* **2008**, *78*, 161408.
(96) Ziroff, J.; Gold, P.; Bendounan, A.; Forster, F.; Reinert, F. *Surf. Sci.* **2009**, *603*, 354–358.
(97) Mehlhorn, M.; Simic-Milosevic, V.; Jaksch, S.; Scheier, P.; Morgenstern, K. *Surf. Sci.* **2010**, *604*, 1698–1704.
(98) Petersen, L.; Laitenberger, P.; Laegsgaard, E.; Besenbacher, F. *Phys. Rev. B* **1998**, *58*, 7361.
(99) Reinert, F.; Nicolay, G.; Schmidt, S.; Ehm, D.; Hüfner, S. *Phys. Rev. B* **2001**, *63*, 115415.
(100) Schouteden, K.; Haesendonck, C. V. *J. Phys.: Condens. Matter* **2010**, *22*, 255504.
(101) Joachim, C. *New J. Chem.* **1991**, *15*, 223–229.
(102) Yokota, K.; Taniguchi, M.; Tsutsui, M.; Kawai, T. *J. Am. Chem. Soc.* **2011**, *132*, 17364–17365.
(103) Song, H.; Reed, M. A.; Lee, T. *Adv. Mater.* **2011**, *23*, 1583–1608.
(104) Nishikawa, A.; Tobita, J.; Kato, Y.; Fujii, S.; Suzuki, M.; Fujihira, M. *Nanotechnology* **2007**, *18*, 424005.
(105) Solomon, G. C.; Reimers, J. R.; Hush, N. S. *J. Chem. Phys.* **2005**, *122*, 224502.
(106) Fenter, P.; Eberhardt, A.; Eisenberger, P. *Science* **1994**, *266*, 1216–1218.
(107) Poirier, G. E. *Langmuir* **1997**, *13*, 2019–2026.
(108) Roper, M. G.; Skegg, M. P.; Fisher, C. J.; Lee, J. J.; Dhanak, V. R.; Woodruff, D. P.; Jones, R. G. *Chem. Phys. Lett.* **2004**, *389*, 87–91.
(109) Voznyy, O.; Dubowski, J. J.; Yates, J. T.; Maksymovych, P. *J. Am. Chem. Soc.* **2009**, *131*, 12989–12993.
(110) Kautz, N. A.; Kandel, S. A. *J. Am. Chem. Soc.* **2008**, *130*, 6908–6909.
(111) Cossaro, A.; Mazzarello, R.; Rousseau, R.; Casalis, L.; Verdini, A.; Kohlmeyer, A.; Floreano, L.; Scandolo, S.; Morgante, A.; Klein, M. L.; Scoles, G. *Science* **2008**, *321*, 943–946.
(112) Torres, E.; Biedermann, P. U.; Blumenau, A. T. *Int. J. Quantum Chem.* **2009**, *109*, 3466–3472.
(113) Frohn, J.; Wolf, J. F.; Besocke, K.; Teske, M. *Rev. Sci. Instrum.* **1989**, *60*, 1200–1201.
(114) Ferris, J. H.; Kushmerick, J. G.; Johnson, J. A.; Youngquist, M. G. Y.; Kessinger, R. B.; Kingsbury, H. F.; Weiss, P. S. *Rev. Sci. Instrum.* **1998**, *69*, 2691–2695.
(115) Bumm, L. A.; Arnold, J. J.; Charles, L. F.; Dunbar, T. D.; Allara, D. L.; Weiss, P. S. *J. Am. Chem. Soc.* **1999**, *121*, 8017–8021.
(116) Frisch, M. J.; et al. *Gaussian 09*, Revision A.02; Gaussian Inc.: Wallingford, CT, 2009.